International Journal of Nanomedicine

Dovepress
Taylor & Francis Group

Open Access Full Text Article

ORIGINAL RESEARCH

Lactobacillus johnsonii-Derived Extracellular Vesicles Ameliorate Alcohol-Exacerbated Experimental Autoimmune Prostatitis by Inhibiting M1 Macrophage Polarization

Qiqi Zhu[1,2,*], Yifu Liu[3,*], Weiwen Hu[4,*], Ying Liu[5], Shengqiang Fu[6], Wenjie Xie[1,2], Ji Liu[7], Yunbing Xiong[1,2], Ting Sun[1,2], Binbin Gong[1,2]

[1]Department of Urology, The First Affiliated Hospital, Jiangxi Medical College, Nanchang University, Nanchang, Jiangxi, People's Republic of China; [2]Jiangxi Provincial Key Laboratory of Urinary System Diseases, Department of Urology, the First Affiliated Hospital, Jiangxi Medical College, Nanchang University, Nanchang, Jiangxi, People's Republic of China; [3]Department of Urology, The Second Affiliated Hospital, Hengyang Medical School, University of South China, Hengyang, Hunan, People's Republic of China; [4]Department of Ophthalmology, The First Affiliated Hospital, Jiangxi Medical College, Nanchang University, Nanchang, Jiangxi, People's Republic of China; [5]Department of Pathology, The First Affiliated Hospital, Jiangxi Medical College, Nanchang University, Nanchang, Jiangxi, People's Republic of China; [6]Department of Anesthesiology, The First Affiliated Hospital, Jiangxi Medical College, Nanchang University, Nanchang, Jiangxi, People's Republic of China; [7]Department of Transplantation, Jiangxi Provincial People's Hospital, The First Affiliated Hospital of Nanchang Medical College, Nanchang, Jiangxi, People's Republic of China

*These authors contributed equally to this work

Correspondence: Ting Sun; Binbin Gong, Department of Urology, The First Affiliated Hospital, Jiangxi Medical College, Nanchang University, Nanchang, Jiangxi, People's Republic of China, Tel +86 13879196600; +86 15270993912, Email 361439919033@email.ncu.edu.cn; ndyfy05944@ncu.edu.cn

Purpose: This study investigated how alcohol exacerbated chronic prostatitis/chronic pelvic pain syndrome (CP/CPPS) and assessed gut microbiota-targeted therapeutic strategies.

Methods: An alcohol-treated experimental autoimmune prostatitis (EAP) mouse model was established to evaluate the exacerbating effect of alcohol on CP/CPPS. The involvement of gut microbiota was assessed by antibiotic depletion and fecal microbiota transplantation (FMT). 16S rRNA sequencing was applied to profile microbial alterations, particularly the abundance of *Lactobacillus johnsonii* (*L. john*). Oral administration of live *L. john* or intravenous injection of *Lactobacillus johnsonii*-derived extracellular vesicles (LjEVs) was tested as therapeutic interventions. Mechanistic studies were conducted in lipopolysaccharide (LPS)-stimulated RAW 264.7 macrophages using transcriptomics, qRT-PCR, Western blot, and flow cytometry.

Results: Alcohol consumption aggravated pelvic tactile hypersensitivity and prostatic inflammation, increased pro-inflammatory cytokines (IL-1β, IL-6, TNF-α), and promoted M1 macrophage polarization in EAP mice. Fecal microbiota transplantation from alcohol-fed EAP mice reproduced the aggravated phenotype, confirming that gut microbiota mediates this effect. Alcohol specifically reduced the relative abundance of *L. john*. Oral *L. john* or intravenous LjEVs alleviated tactile hypersensitivity and inflammation, and inhibited M1 macrophage polarization in alcohol-fed EAP mice. In vitro, LjEVs were internalized by macrophages, suppressed LPS-induced M1 macrophage polarization and pro-inflammatory gene expression, and inhibited TNF-α/NF-κB signaling. Exogenous TNF-α reversed the inhibitory effects of LjEVs on M1 macrophage polarization.

Conclusion: Alcohol exacerbated EAP by reducing *L. john*, which in turn promoted prostatic M1 macrophage polarization via the TNF-α/NF-κB pathway. Supplementation with *L. john* or LjEVs ameliorated the disease by suppressing this pathway, offering a microbiota-targeted therapy for alcohol-aggravated CP/CPPS.

Keywords: chronic prostatitis/chronic pelvic pain syndrome, alcohol, *Lactobacillus johnsonii*, extracellular vesicles, macrophage polarization

https://doi.org/10.2147/IJN.S596237
Received: 14 January 2026
Accepted: 12 May 2026
Published: 3 June 2026

Introduction

Chronic prostatitis/chronic pelvic pain syndrome (CP/CPPS) ranks among the most prevalent urological disorders in young and middle-aged males worldwide, affecting 4.5–10% of the global male population—nearly 50% of whom develop symptoms during their lifetime, typically manifesting as pelvic pain syndromes (genital, ejaculatory, abdominal), lower urinary tract symptoms (LUTS), and erectile dysfunction, collectively compromising quality of life.[1–3] The precise pathogenesis of CP/CPPS remains incompletely characterized, potentially involving multifactorial interactions among pelvic floor myofascial dysfunction, immunological aberrations, dietary influences, urine reflux phenomena, and endocrine dysregulation.[4]

The immune dysregulation hypothesis is well-established in CP/CPPS etiology. Studies show elevated levels of IFN-γ, IL-17, IL-1β, and IL-8, along with increased $CD4^+$ T cells and macrophages in patient semen.[5] Mouse models corroborate these findings, demonstrating enhanced macrophage infiltration in prostate tissue and dorsal root ganglia that drives CP/CPPS.[6,7] Macrophage depletion significantly alleviates pelvic pain,[7] while recent research shows CXCL10 promotes macrophage recruitment to worsen CP/CPPS.[4] Moreover, inhibiting M1 macrophage activation markedly reduces inflammation and pain.[8] These findings collectively establish that macrophage infiltration and pro-inflammatory phenotype activation are closely linked to CP/CPPS development and progression.

Globally, the consumption of alcoholic beverages continues to present a considerable public health challenge. The detrimental effects of alcohol consumption, which impact nearly all organ systems and are linked to a spectrum of inflammatory diseases such as hepatitis, pancreatitis, neuroinflammation, and atherosclerosis,[9–13] are mediated through mechanisms involving macrophage infiltration and M1 polarization.[13,14] Epidemiological studies indicate that alcohol consumption is identified as a potential risk factor for CP/CPPS and adversely affects its prognosis.[15,16] Previous research indicates that alcohol consumption could aggravate CP/CPPS through various potential mechanisms. Clinical evidence shows that alcohol-drinking patients have higher symptom scores and elevated Th17 cells, associated with reduced gut short-chain fatty acids.[17] Mechanistically, alcohol exacerbates EAP by promoting Th17 differentiation via gut microbiota-driven cholesterol biosynthesis, and by activating the PI3K/AKT/mTOR pathway to drive Th1 differentiation.[18,19] Despite these evidences, the underlying pathophysiology linking alcohol to CP/CPPS is still unclear.

As the connection between gut microbiota and CP/CPPS has garnered increasing attention, the concept of the "gut-prostate axis" has emerged, offering a novel perspective for understanding the pathogenesis of the disease.[20,21] Mechanistically, gut dysbiosis drives prostate inflammation through reduced short-chain fatty acids such as propionate, which disrupt Th17/Treg immune homeostasis via the GPR43-HDAC6 axis, as well as through gut microbiota-derived metabolites like putrescine, which modulate Th17 differentiation via the TRAF6/JAK2/STAT3 signaling pathway.[22,23] Probiotics are live microorganisms that colonize the host's intestinal tract and exert beneficial effects by participating in immune regulation, combating pathogenic bacteria, and enhancing intestinal barrier function.[24] *Lactobacillus johnsonii* (*L. john*) is a typical intestinal probiotic. Recent studies have demonstrated its potential therapeutic value in various inflammatory diseases, including inflammatory bowel disease, pneumonia, and alcohol-associated liver disease (ALD).[25–27] Bacterial extracellular vesicles (BEVs) are spherical, bilayered membranous vesicles produced by parent bacteria. They are enriched with nucleic acids, proteins, and lipids, and play a crucial role in host-microbe interactions.[28] Notably, BEVs offer distinct advantages over live probiotics, including excellent stability, a superior safety profile that avoids risks associated with live bacteria in vulnerable populations, and the potential for effective systemic delivery.[29,30] Several studies have demonstrated that extracellular vesicles derived from *Lactobacillus johnsonii* (LjEVs) can alleviate colitis, diarrhea and osteoarthritis by modulating macrophage polarization;[31–33] however, their role in CP/CPPS remains unknown. Given that alcohol exposure significantly reduces gut *Lactobacillus* abundance in the EAP mouse model and that LjEVs possess immunomodulatory properties,[18,31] we hypothesized that LjEVs might protect against alcohol-exacerbated EAP by regulating macrophage polarization.

To delineate the role of alcohol in CP/CPPS, we employed an EAP mouse model replicating human disease characteristics. Alcohol was found to worsen inflammation and pain in EAP mice, linked to increased M1 macrophage infiltration and pro-inflammatory cytokine levels. Gut microbiota analysis revealed alcohol-induced dysbiosis, and 16S rRNA sequencing pinpointed *L. john* as a key candidate. Intervention with *L. john* or its extracellular vesicles (EVs) counteracted the aggravating effects of alcohol. The underlying mechanism involves the inhibition of M1 macrophage

polarization and TNF-α/NF-κB signaling pathway by LjEVs, as established through both in vitro and in vivo experiments. Thus, our work identifies *L. john* and its EVs as mitigating agents in alcohol-aggravated EAP, acting through suppression of M1 macrophage polarization and the TNF-α/NF-κB pathway.

Materials and Methods

Bacterial Strain and Culture

As previously described,[34,35] *Lactobacillus johnsonii* was cultured in de Man, Rogosa and Sharpe (MRS) medium at 37°C for 24 hours under an atmosphere of 10% H_2, 10% CO_2, and 80% N_2. Bacterial quantification was performed by enumerating colony-forming units (CFU) following plating on agar plates. After centrifugation at 6000 rpm for 5 minutes at 4°C, the bacterial pellet was washed three times with sterile phosphate-buffered saline (PBS). The washed cells were typically cryopreserved in sterile PBS containing 20% glycerol at a final concentration of 1×10^{10} CFU/mL.

Isolation and Identification of LjEVs

Extracellular vesicles (EVs) were isolated from the culture supernatant of *L. john* strain via ultracentrifugation as described in references.[32] Approximately 500 mL of *L. john* culture at logarithmic phase was centrifuged at 8000 × g for 30 minutes. The supernatant was collected and centrifuged at 20,000 × g for 45 minutes, then filtered through a 0.22 μm filter. The filtrate was centrifuged at 120,000 × g for 2 hours at 4°C using an SW 32 Ti rotor (Beckman Coulter, Fullerton, CA, USA). The pellet was resuspended in PBS and the centrifugation was repeated once. The final pellet was collected in PBS. EVs presence was confirmed by transmission electron microscopy (TEM), and their size range and concentration were determined via nano-flow cytometry (nFCM).

Animals and Treatments

Male non-obese diabetic (NOD)/ShiLtJ mice aged 6–8 weeks were purchased from Jiangsu GemPharmatech Co., Ltd. (Nanjing, China). All mice were housed in the specific pathogen-free (SPF) animal laboratory of the First Affiliated Hospital of Nanchang University, and after a one-week acclimation period prior to treatment, they were randomly assigned to different treatment groups. All animal experiments comply with guidelines for the care and use of laboratory animals. The experimental protocols were approved by the Animal Ethics Committee of the First Affiliated Hospital of Nanchang University (CDYFY-IACUC-202311QR006).

As described in the previous study,[36] the EAP mice had been established. Specifically, prostate tissues were excised from Sprague-Dawley rats, rinsed under sterile conditions, and homogenized. The homogenate was then centrifuged, and the supernatant was collected as prostate antigen. Subsequently, prostate antigen (300 μg per mouse) or PBS was fully emulsified with an equal volume of complete Freund's adjuvant (Sigma-Aldrich), and the emulsions were administered to mice in the EAP group and control group, respectively. According to the experimental protocol, immunization was performed via subcutaneous injection of the emulsion at three sites on day 0 and day 28: the base of the tail (0.050 mL), bilateral footpads (0.025 mL per pad), and shoulders (0.050 mL). On day 42, feces were collected prior to euthanizing the mice.

To evaluate the effect of alcohol on the prostate of mice, a 5-day liquid diet adaptation period was initiated on day 27. Subsequently, from day 32 onward, mice in the control+alcohol and EAP+alcohol group were given a 5% (vol/vol) ethanol Lieber-DeCarli diet for 10 days (ad libitum oral feeding), plus a single binge feeding of 31.5% (vol/vol) ethanol administered via gavage on day 42 at a dose of 5 g alcohol per kilogram of body weight. In contrast, mice in the control and EAP group were fed an isocaloric control diet. The detailed alcohol feeding protocol has been documented in previous literature.[37]

To evaluate whether alcohol promotes CP/CPPS in a gut microbiota-dependent manner, we prepared microbiota-depleted mice. These mice were provided with sterile drinking water containing broad-spectrum antibiotics (Ampicillin, 1 g/L; metronidazole, 1 g/L; neomycin sulfate, 1 g/L; vancomycin, 0.5 g/L) for two weeks. Notably, three days before model induction, the antibiotic-containing drinking water was replaced with sterile regular drinking water for mice to ensure complete clearance of antibiotics. Subsequently, mice in the (FMT)EAP group and (FMT)EAP+Alcohol group received gut microbiota from mice of the EAP group and EAP+Alcohol group, respectively. To prepare the gut

microbiota suspension, feces were collected from donor mice after the second immunization and resuspended in sterile PBS at a concentration of 100 mg feces per 1 mL solution. The suspension was then centrifuged at 500 × g for 1 minute to collect the supernatant, and bacterial counts were determined using the bacterial colony counting method. According to the experimental protocol, each mouse was administered 200 μL of the microbiota suspension (2×10^8 CFU) via gavage every other day, starting from the first immunization until euthanasia.[36]

To investigate the role of *L. john* in CP/CPPS exacerbated by alcohol, after immunization on day 28, mice in the EAP +alcohol+*L. john* group were administered 200 μL of sterile PBS containing 1×10^9 CFU of *L. john* via oral gavage once daily until one day before euthanasia. In contrast, mice in the EAP group and EAP+alcohol group received an equal volume of sterile PBS.

To examine the role of LjEVs in alcohol-exacerbated CP/CPPS, after immunization on day 28, each mouse in the EAP+Alcohol+LjEVs group received LjEVs at a dose of 1×10^9 particles (normalized from a rat study based on body weight) via tail vein injection once a week until one day before euthanasia, while mice in the EAP+alcohol group received an equal volume of sterile PBS.[38]

Behavior Testing

Von Frey filaments were used to quantify tactile allodynia in the lower abdomen of mice (near the prostate region): after the mice were acclimated to an individual plastic chamber with a stainless steel mesh floor for 30 minutes, five types of filaments (0.04, 0.16, 0.4, 1.0, and 4.0 g) were applied to different points in the target area (1–2 seconds per stimulation, 5-second interval, 10 stimulations per filament).[39] Positive responses included sudden abdominal contraction, licking/scratching the stimulated area, or jumping. The positive response rate and the 50% pain threshold determined by the up-down method were used as evaluation indicators.[40]

Hematoxylin–Eosin (H&E) Staining

After anesthesia, the mice were euthanized by cervical dislocation. The prostate tissues were isolated and fixed in 4% paraformaldehyde for 48 hours. Following gradient dehydration with ethanol, transparency treatment with xylene, and paraffin embedding, 5-μm-thick sections were prepared. H&E staining was performed using special reagents provided by Servicebio (Wuhan, China). After standard dehydration, the prostate tissue sections were mounted with neutral resin. Finally, the sections were observed under an optical microscope to analyze the pathological changes of the prostate tissue. The inflammation of prostate tissue was evaluated according to the following criteria: 0, no signs of inflammation; 1, mild but distinct perivascular cuff-like infiltration of monocytes or vascular proliferation; 2, moderate perivascular cuff-like infiltration of monocytes with aggravated vascular proliferation; 3, significant perivascular cuff-like infiltration accompanied by hemorrhage, as well as extensive infiltration of a large number of monocytes in the stroma or parenchyma.[41]

Immunohistochemistry and Immunofluorescence

For immunohistochemical staining of mouse prostate paraffin sections, the samples underwent sequential dewaxing, hydration, and antigen retrieval. Subsequently, sections were incubated with 3% hydrogen peroxide at room temperature for 25 minutes in the dark, rinsed three times with PBS (pH 7.4), and blocked with 3% BSA for 30 minutes. They were then incubated overnight at 4°C with primary anti-CD45 antibody (1:200, GB113886, Servicebio) in a humid chamber. After PBS washes, HRP-conjugated secondary antibody (1:200, GB23303, Servicebio) was applied for 50 minutes at room temperature. DAB staining was microscopically monitored and terminated with tap water. Nuclei were counter-stained with hematoxylin, followed by differentiation and bluing. Sections were dehydrated, cleared, mounted, and examined under a bright-field microscope.

For immunofluorescence staining, dewaxed and antigen-retrieved paraffin sections were subjected to a sequential Tyramide Signal Amplification (TSA) protocol. Sections were first incubated with anti-CD86 (1:200, DF6332, Affinity), followed by an HRP-conjugated secondary antibody and the TYR-488 (IF488) tyramide reagent. After antibody stripping via microwave retrieval, sections were then incubated with anti-CD206 (1:200, 18704-1-AP, Proteintech), followed by the corresponding HRP-conjugated secondary antibody and the TYR-555 (IF555) tyramide reagent. Following DAPI staining, signals were detected under a fluorescence microscope in a dark room.

Quantitative Real-Time PCR and Enzyme-Linked Immunosorbent Assay

cDNA was obtained via reverse transcription with the First-Strand cDNA Synthesis Kit (TIANGEN, China) after RNA extraction. A 20 μL reaction system containing cDNA, primer (Table S1, supplementary information), and qPCR reaction buffer was configured following the instructions of SYBR Green qPCR Master Mix (Servicebio, China). All qPCR assays were performed with a minimum of three independent biological replicates, and each sample was run in triplicate.

The levels of TNF-α (E-MSEL-M0002, Elabscience, China), IL-1β (E-MSEL-M0003, Elabscience, China), and IL-6 (E-MSEL-M0001, Elabscience, China) in mouse serum were detected using enzyme-linked immunosorbent assay (ELISA) kits according to the manufacturers' instructions, followed by statistical analysis.

Western Blotting

After the samples were treated with protein lysis buffer (Solarbio, China) supplemented with protease and phosphatase inhibitors, the supernatant was collected and the protein concentration was determined using a BCA protein assay kit. Proteins were separated by 10% SDS-PAGE gel electrophoresis and then transferred to a PVDF membrane using a Bio-Rad semi-dry transfer system. The PVDF membrane was blocked with 5% BSA at room temperature for 1 hour, followed by overnight incubation at 4°C with the corresponding primary antibodies (TNF, 1:1000, 17590-1-AP, Proteintech; NF-κB p65, 1:1000, 380172, Zenbio; Phospho-NF-κB p65, 1:1000, 310013, Zenbio; β-actin, 1:10000, 81115-1-RR, Proteintech). After washing with TBST, the PVDF membrane was incubated with the secondary antibody (1:10000, SA00001-2, Proteintech) at room temperature for 1 hour. Target proteins were visualized by exposure with high-sensitivity chemiluminescent solution, and protein bands were quantified using ImageJ software. All Western blot experiments were performed with three independent biological replicates.

16S rRNA Sequencing

Mouse fecal samples were immediately frozen after collection and sent to OE biotech Co., Ltd. (Shanghai, China) for 16S rRNA gene sequencing. Genomic DNA was extracted from the samples using the MagPure Soil DNA LQ Kit (Magan) following the manufacturer's instructions, and stored at −20°C after detecting its concentration and purity. Using the extracted genomic DNA as a template, the V3-V4 variable region of the bacterial 16S rRNA gene was amplified by PCR with Barcode-specific primers and Takara Ex Taq high-fidelity enzyme, using universal primers 343F (5′-TACGGRAGGCAGCAG-3′) and 798R (5′-AGGGTATCTAATCCT-3′), for bacterial diversity analysis. QIIME 2 software was used for α and β diversity analysis: α diversity was evaluated by indicators such as ACE, Chao1 and Shannon indices, while β diversity was assessed by principal coordinate analysis (PCoA).

Cell Culture and in vitro Cell Uptake Assay

RAW 264.7 cells were cultured in high-glucose Dulbecco's modified Eagle's medium (DMEM) supplemented with 10% fetal bovine serum (FBS) and 100 U/mL penicillin-streptomycin. The cell culture was conducted at 37°C in a humidified incubator with a 5% CO_2 atmosphere. To observe the uptake of extracellular vesicles by RAW 264.7 cells, 1 μL of diluted Dil dye was co-incubated with 1 mL of LjEVs at 4°C for 6 hours in the dark. Unbound dye in the resulting sample was removed by ultracentrifugation (100,000 × g, 4°C, 60 minutes). Subsequently, RAW 264.7 cells were incubated with LjEVs@Dil or free Dil at 37°C for 12 hours. After incubation, cell nuclei were stained with 4′,6-diamidino-2-phenylindole (DAPI, Boster, Wuhan, China), and the cytoskeleton was stained with fluorescein isothiocyanate (FITC)-labeled phalloidin (Beyotime, Shanghai, China). The fixed cells were then observed and imaged using a confocal laser scanning microscope (Leica, Germany).

Distribution of LjEVs in vivo

Detailed experimental procedures are described in previous studies.[42] ICG was dissolved in normal saline containing 4% (v/v) DMSO, mixed with isolated EVs, and incubated at 4 °C for 6 h with gentle agitation. Unbound dye was then removed by ultracentrifugation at 100,000 × g for 60 minutes at 4 °C. After model establishment, mice were randomly assigned to two groups, and each mouse received either EVs@ICG or free ICG via tail vein injection. Prior to imaging,

mice were anesthetized with 2% isoflurane. The in vivo fluorescence distribution was evaluated 12 hours post-injection using an imaging system from MILabs (Netherlands). Additionally, ex vivo imaging was also performed on major isolated organs for precise signal localization.

Flow Cytometry

RAW 264.7 cells were seeded at a density of 1×10^6 cells per well. The LPS+LjEVs and LPS+LjEVs+TNF-α groups were first co-incubated with 10 μg/mL LjEVs (the latter group also received 100 ng/mL recombinant TNF-α) for 12 hours, while the Control and LPS groups received an equal volume of PBS. Subsequently, the LPS, LPS+LjEVs and LPS+LjEVs+TNF-α groups were treated with 1 μg/mL LPS for an additional 12 hours, and the Control group was again supplemented with PBS. After treatment, the culture medium was aspirated, 1 mL PBS was added to resuspend and collect the cells, which were then centrifuged at 5000 rpm for 5 minutes. After discarding the supernatant, the cells were resuspended in 100 μL PBS, and antibodies against CD86 (560582, BD Biosciences) and CD163 (155305, BioLegend) were added, followed by incubation at 4°C in the dark for 30 minutes. After staining, the cells were washed twice with cold PBS, resuspended in 500 μL PBS, detected using an Agilent flow cytometer, and the data were analyzed with NovoExpress software. Flow cytometry was performed with three independent biological replicates.

Nitric Oxide (NO) Detection

Nitric oxide (NO) detection was performed using the S0021S kit purchased from Beyotime Biotechnology. The detailed protocol was as follows: First, Griess Reagent I and II were taken out and equilibrated to room temperature. Subsequently, the standard solution was serially diluted to the concentration range of 1–100 μM using the same solvent as the test samples. Then, 50 μL of each standard or sample was added to the corresponding wells of a 96-well microplate. Afterwards, 50 μL of Griess Reagent I and 50 μL of Griess Reagent II were sequentially added to each well. After the reaction, the absorbance of each well was measured at a wavelength of 540 nm using a microplate reader. Finally, the concentration of NO in the test samples was calculated based on the standard curve constructed from the absorbance values of the standard solutions. All NO detection assays were performed with three independent biological replicates, and each sample was run in triplicate.

Statistical Analysis

All statistical analyses were carried out using GraphPad Prism 9.0.0 software (San Diego, CA, USA). Sample sizes (n = 6 per group) are consistent with those commonly used in comparable CP/CPPS studies and adhere to the 3R principle. Normality of distribution was assessed using the Shapiro–Wilk test. For comparisons between two groups, the two-tailed Student's *t*-test was applied for normally distributed data, otherwise the Mann–Whitney *U*-test was used. For comparisons among three or more groups, one-way analysis of variance (ANOVA) was performed for normally distributed data, otherwise the Kruskal–Wallis test was used. A p-value < 0.05 was considered statistically significant.

Results

Alcohol Consumption Aggravates Prostate Inflammation and Promotes M1 Macrophage Polarization in EAP Mice

To model the impact of alcohol on CP/CPPS, EAP mice were subjected to a 10-day Lieber-DeCarli liquid diet containing ethanol, followed by a single binge ethanol feeding (Figure 1A).[37] Body weight did not differ significantly among any of the groups, regardless of alcohol intake (Figure 1B). Compared to the Control group, EAP mice exhibited increased response frequency to mechanical stimulation of the pelvic region and a significantly reduced 50% response threshold. This tactile allodynia was further exacerbated by alcohol administration (Figure 1C and D). No such changes were observed between the Control and Control+Alcohol groups (Figure 1C and D). Given the sparse inflammatory infiltration previously reported in the ventral lobe,[43] the anterior and dorsolateral lobes of the prostate were selected for histopathological assessment. H&E staining revealed more severe inflammation in the prostate of the EAP+Alcohol group compared to the EAP group. No inflammatory infiltration was observed in the Control or Control+Alcohol groups

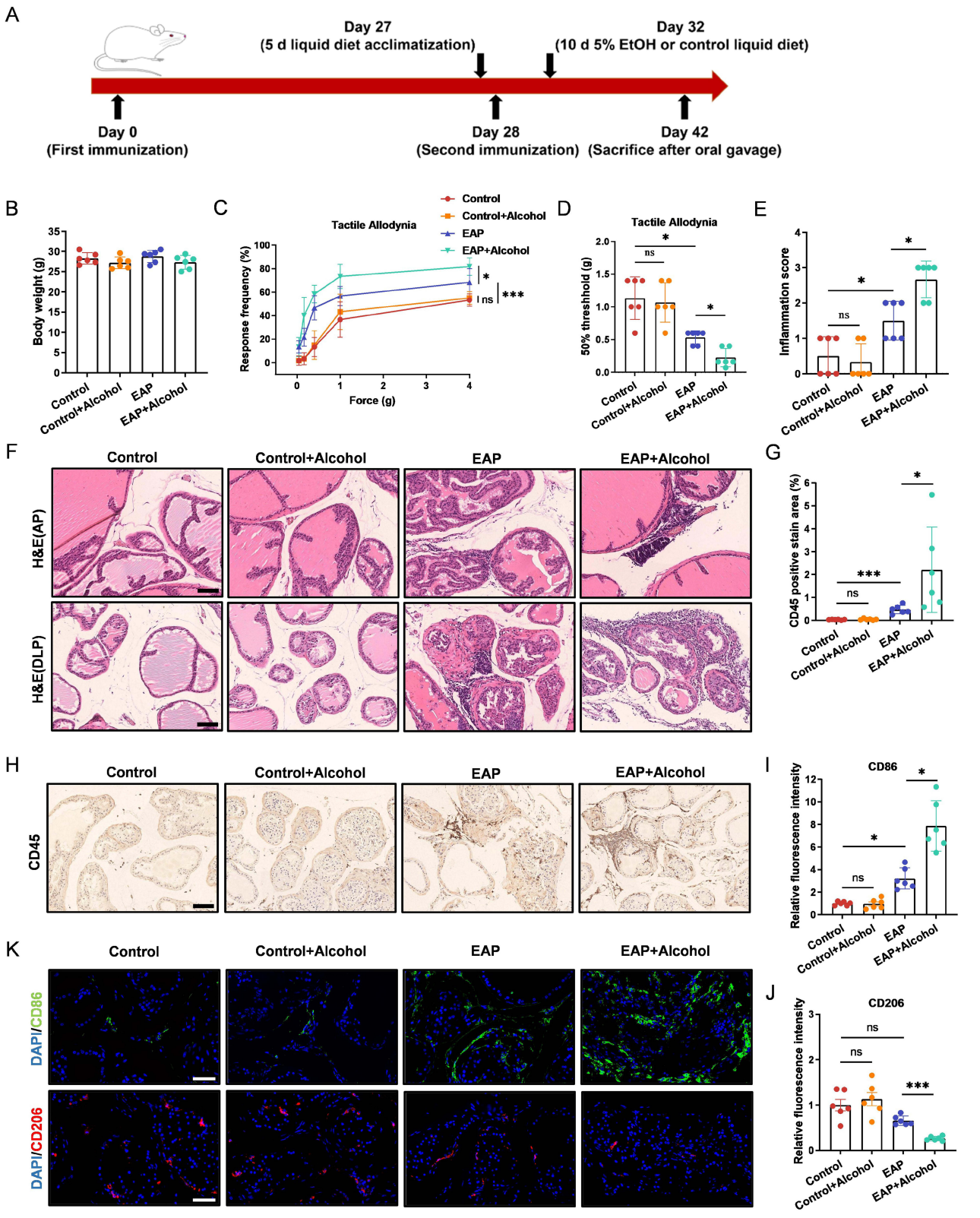

Figure 1 Alcohol consumption aggravates prostate inflammation and promotes M1 macrophage polarization in EAP mice. (**A**) Schematic of the experimental timeline for EAP induction and alcohol intervention. (**B**) The body weights of mice in the Control, Control+Alcohol, EAP, and EAP+Alcohol groups. (**C** and **D**) Response frequency to mechanical stimuli and the 50% mechanical withdrawal threshold. (**E**) Prostate inflammation score. (**F**) H&E staining of the anterior and dorsolateral prostate. Scale bars, 100 μm. (**G**) Percentage of CD45-positive staining in prostate immunohistochemistry. (**H**) Immunohistochemical staining of CD45 in prostate tissues. Scale bars, 100 μm. (**I-J**) Relative fluorescence intensity of CD86 and CD206 in prostate tissue. (**K**) Immunofluorescence staining of CD86 and CD206 in prostate tissue. Scale bars, 50 μm. Data are presented as mean ± SD (n = 6 for B-K). *, $p < 0.05$; ***, $p < 0.001$.

Abbreviation: ns, not significant.

https://doi.org/10.2147/IJN.S596237

(Figure 1E and F). CD45, a pan-leukocyte biomarker, was selected to assess inflammation due to its reported upregulation in CP/CPPS models.[44] Consistent with this, our study confirmed a significant increase in $CD45^+$ leukocytes in the EAP model, which was further amplified by alcohol intake (Figure 1G and H).

Levels of pro-inflammatory cytokines (IL-1β, IL-6, TNF-α) in mouse serum and prostate tissue were evaluated by ELISA and qRT-PCR, respectively. Compared to the Control group, cytokine levels were significantly elevated in the EAP group and further increased in the EAP+Alcohol group. No difference was observed between the Control and Control+Alcohol groups (Figure S1A and B, supplementary information). Given the reported association between macrophage polarization and CP/CPPS,[8,45] we performed immunofluorescence staining using CD86 and CD206 as markers for pro-inflammatory M1 and anti-inflammatory M2 macrophages, respectively. The results showed that M1 macrophages increased in the prostates of EAP model mice compared to controls. In alcohol-fed EAP mice, M1 macrophages increased further, whereas M2 macrophages decreased (Figure 1I–K). These data demonstrate that alcohol intake exacerbates CP/CPPS in EAP mice and promotes the polarization of macrophages toward the M1 phenotype.

The Gut Microbiota Mediates the Effect of Alcohol on EAP Mice

To investigate whether the effects of alcohol on EAP mice depend on the endogenous gut microbiota, we pretreated mice with an antibiotic cocktail for 14 days prior to modeling to establish a pseudo-germ-free state. Subsequently, we performed fecal microbiota transplantation by orally administering fecal suspensions from EAP mice or alcohol-fed EAP mice to these pseudo-germ-free recipient EAP mice. Consistent with previous findings, oral administration of gut microbiota from alcohol-fed EAP mice increased the frequency of responses to mechanical stimuli in the pelvic region and lowered the mechanical threshold in recipient EAP mice (Figure 2A and B). Similarly, compared to EAP mice that received microbiota from control donors, recipients of gut microbiota from alcohol-fed EAP mice exhibited higher prostate inflammation scores (Figure 2C and D), increased $CD45^+$ leukocyte infiltration (Figure 2E and 2F), and elevated levels of pro-inflammatory cytokines in both serum and prostate tissue (Figure 2I and J). Furthermore, an increase in M1 macrophages and a decrease in M2 macrophages were observed in the prostate (Figure 2G and H). In summary, colonization with gut microbiota from alcohol-fed EAP mice exacerbated both inflammation and pain in recipient EAP mice, suggesting that specific microbes may mediate the detrimental effects of alcohol.

Alcohol Alters the Structure and Composition of the Gut Microbiota in EAP Mice

To investigate the gut microbiota involved in alcohol-aggravated CP/CPPS, fecal samples were collected from mice in the Control, Control+Alcohol, EAP, and EAP+Alcohol groups immediately before euthanasia. Following collection, microbial composition was assessed via 16S rRNA sequencing. We first assessed the α-diversity of the gut microbiota (ACE, Chao1, Observed species, and Shannon indices). No significant difference was found between the Control and EAP groups. However, alcohol intervention significantly reduced α-diversity in mice (Figure 3A–D). Principal coordinate analysis (PCoA) revealed a clear separation between the Control and EAP groups, as well as between samples with and without alcohol exposure, indicating distinct microbial compositions (Figure 3E).

Further analysis at the genus level showed that alcohol intervention reduced the relative abundance of *Lactobacillus*, with no difference observed between the Control and EAP groups (data not shown). At the species level, alcohol similarly decreased the relative abundance of *L. john*, which also did not differ significantly between the Control and EAP groups (Figure 3F and G). To identify microbial taxa significantly altered by alcohol in EAP mice, we performed linear discriminant analysis effect size (LEfSe) analysis comparing the EAP group with the EAP+Alcohol group. *Lactobacillales, Lactobacillaceae*, and *Lactobacillus* all showed high LDA scores (>3) in the EAP group, indicating their enrichment in EAP mice compared to alcohol-treated EAP mice (Figure 3H). The phylogenetic distribution of differentially abundant taxa is displayed in Figure 3I. In summary, the decrease in the relative abundance of *L. john* in the gut after alcohol exposure suggests its potential role as a key bacterium mediating the exacerbation of CP/CPPS in mice by alcohol.

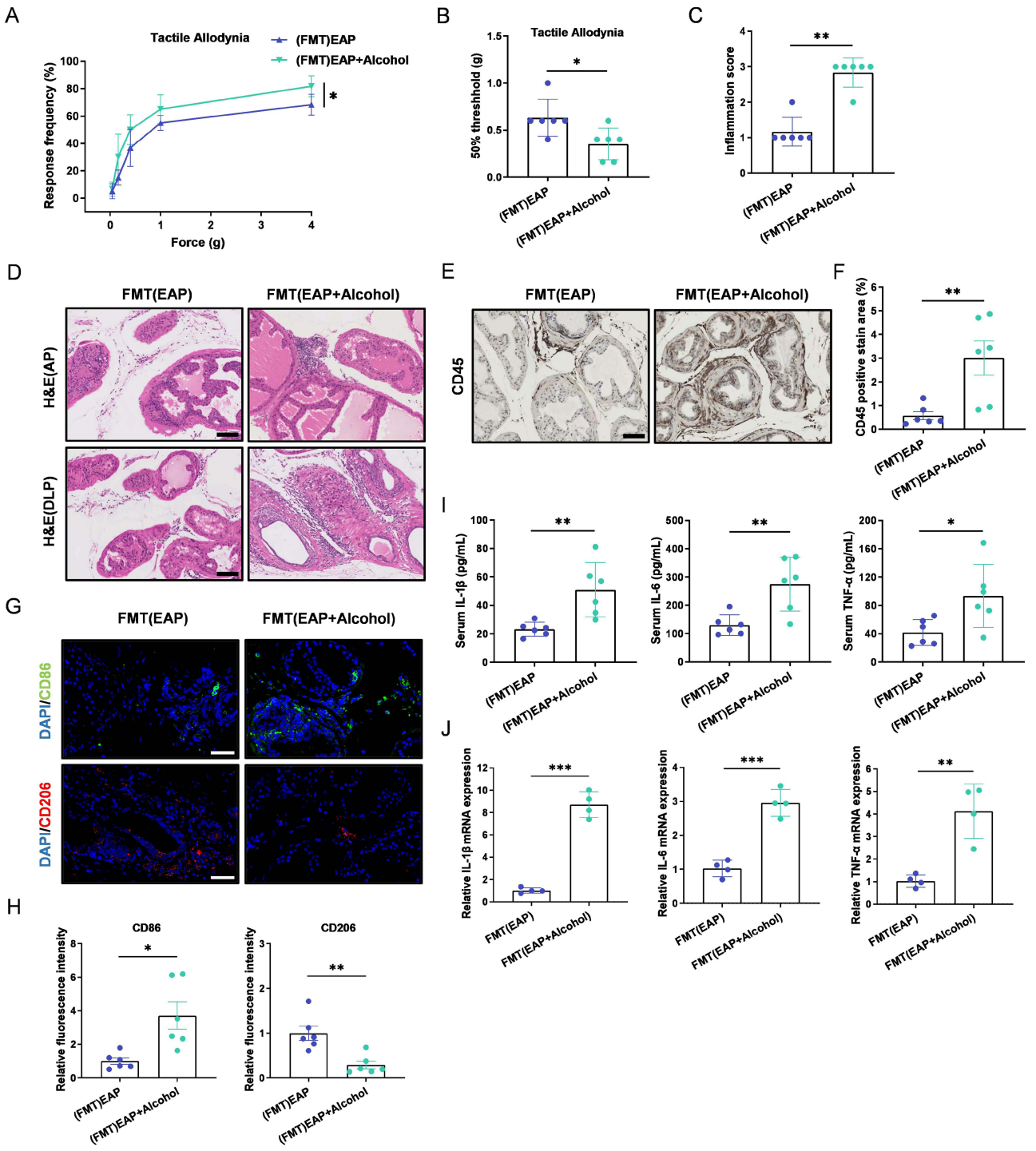

Figure 2 The gut microbiota mediates the effect of alcohol on EAP mice. (**A** and **B**) Response frequency to mechanical stimuli and the 50% mechanical withdrawal threshold. (**C**) Prostate inflammation score. (**D**) H&E staining of the anterior and dorsolateral prostate. Scale bars, 100 μm. (**E**) Immunohistochemical staining of CD45 in prostate tissues. Scale bars, 100 μm. (**F**) Percentage of CD45-positive staining in prostate immunohistochemistry. (**G**) Immunofluorescence staining of CD86 and CD206 in prostate tissue. Scale bars, 50 μm. (**H**) Relative fluorescence intensity of CD86 and CD206 in prostate tissue. (**I**) Pro-inflammatory cytokine levels in serum. (**J**) Pro-inflammatory cytokine mRNA expression in prostate tissues. Data are presented as mean ± SD (n = 6 for A-I, n = 4 for J). *, $p < 0.05$; **, $p < 0.01$; ***, $p < 0.001$.

Transplantation of *L. john* Relieves Prostate Inflammation and Pain in Alcohol-Fed EAP Mice

To investigate the role of *L. john* in CP/CPPS exacerbated by alcohol, after immunization on day 28, mice in the EAP +alcohol+*L. john* group were administered 200 μL of sterile PBS containing 1×10^9 CFU of *L. john* via oral gavage once

https://doi.org/10.2147/IJN.S596237

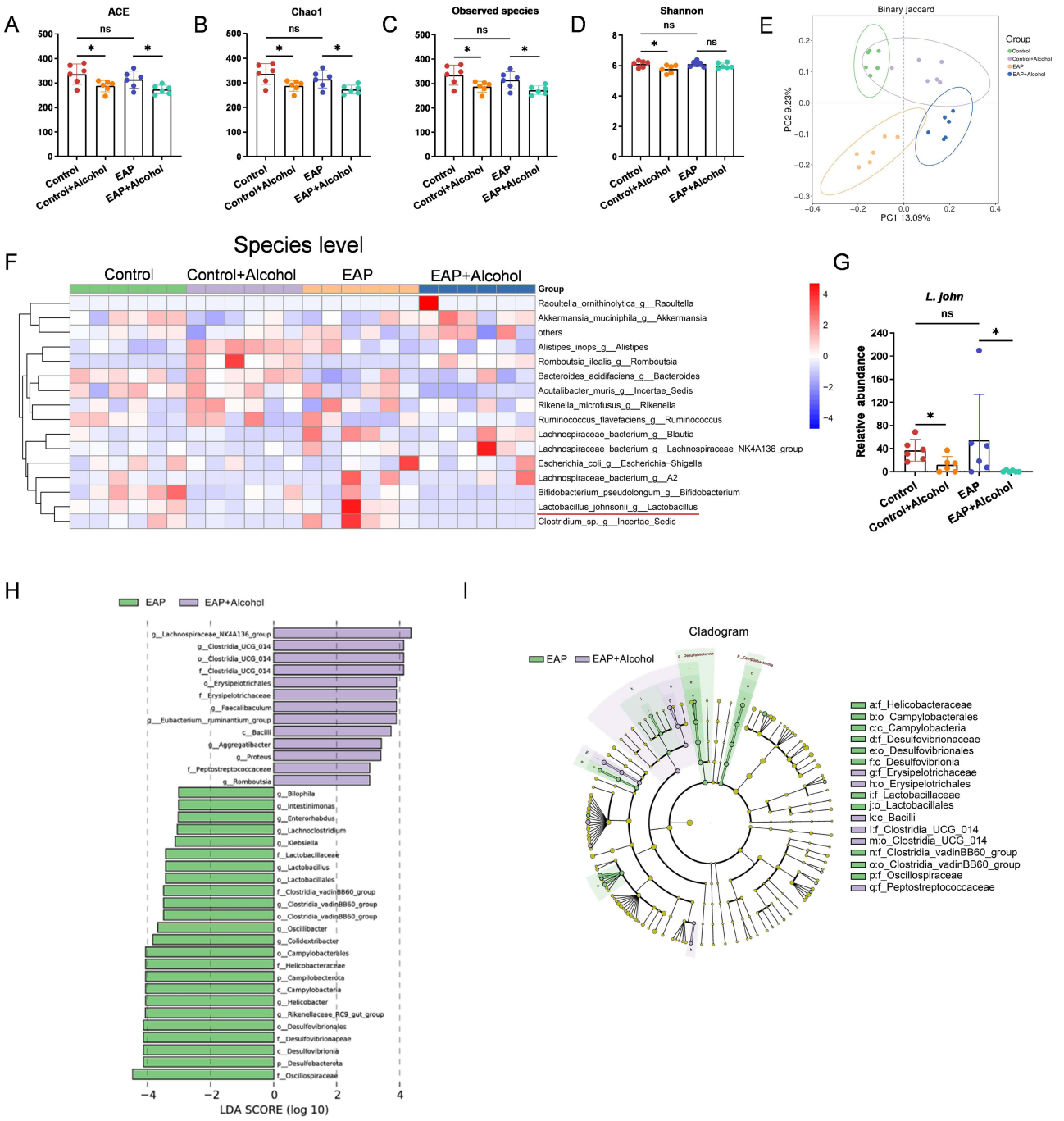

Figure 3 Alcohol alters the structure and composition of the gut microbiota in EAP mice. (**A-D**) The alpha diversity indices (ACE, Chao1, Observed species, Shannon) of bacterial 16S rRNA genes in fecal samples from each group of mice. (**E**) β-Diversity (Principal component analysis) of bacterial 16S rRNA genes in fecal samples from each group of mice. (**F**) At the species level, a heatmap depicting the relative abundance of the top 15 species was constructed to visualize compositional differences across all samples. (**G**) Relative abundance of *L. john* in the fecal microbiota of each mouse group. (**H**) LEfSe analysis of the differentially abundant taxa in the gut microbiota between the EAP and EAP+Alcohol groups. (**I**) Cladogram of differentially abundant bacteria between the EAP and EAP+Alcohol groups. Data are presented as mean ± SD (n = 6 for A-I). *, $p < 0.05$.
Abbreviation: ns, not significant.

daily until one day before euthanasia. Our results indicate that *L. john* treatment effectively ameliorates CP/CPPS in alcohol-exposed EAP mice. Specifically, *L. john* normalized pelvic mechanical sensitivity, as shown by a decreased response frequency and an increased 50% withdrawal threshold (Figure 4A and B). It also attenuated prostate inflammation (Figure 4C and D). Immunohistochemical analyses revealed that oral *L. john* reduced prostate infiltration of $CD45^+$ leukocytes (Figure 4E and F), inhibited M1 macrophage polarization and promotes M2 macrophage polarization

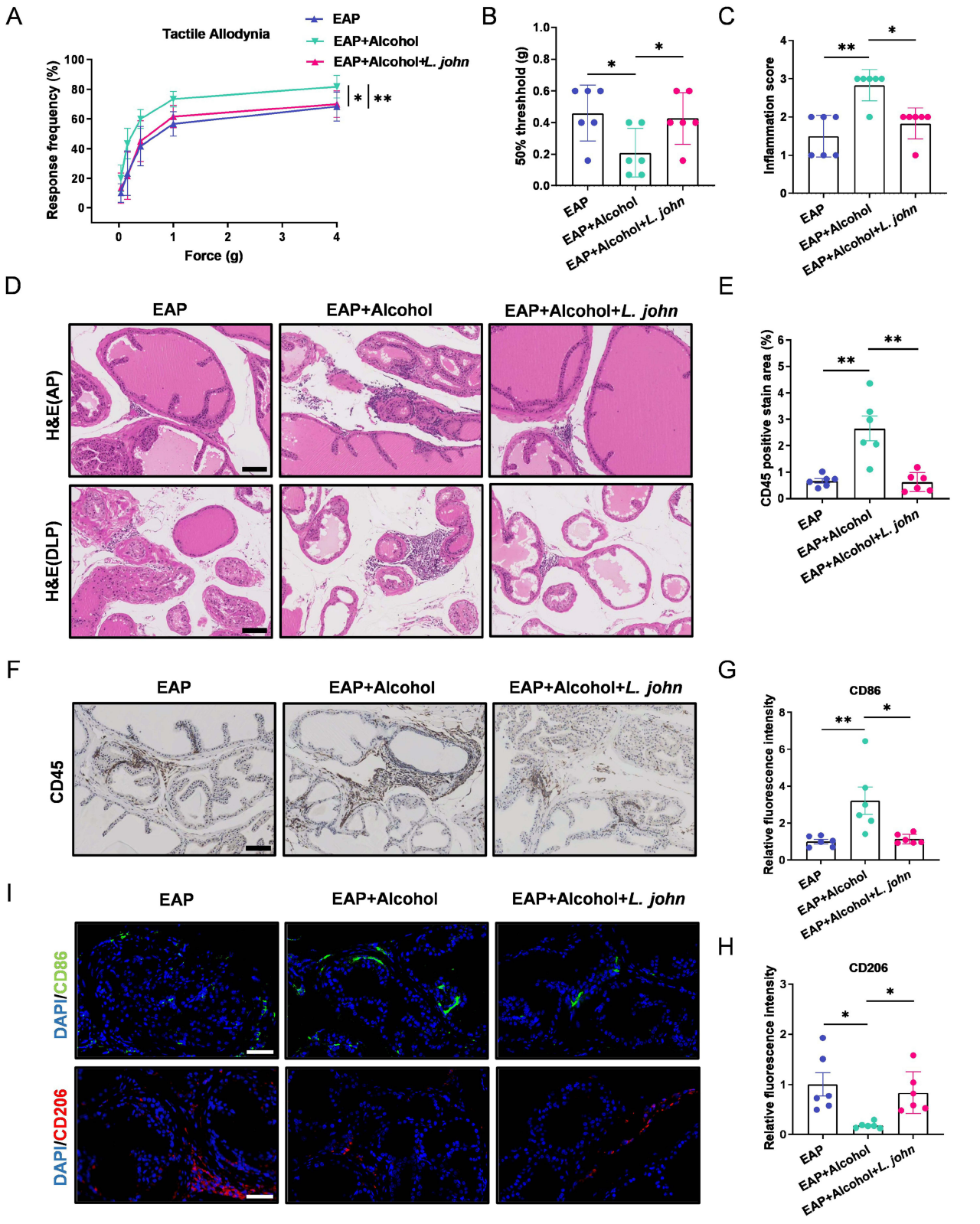

Figure 4 Transplantation of *L. john* relieves prostate inflammation and pain in EAP mice. (**A** and **B**) Response frequency to mechanical stimuli and the 50% mechanical withdrawal threshold. (**C**) Prostate inflammation score. (**D**) H&E staining of the anterior and dorsolateral prostate. Scale bars, 100 μm. (**E**) Percentage of CD45-positive staining in prostate immunohistochemistry. (**F**) Immunohistochemical staining of CD45 in prostate tissues. Scale bars, 100 μm. (**G-H**) Relative fluorescence intensity of CD86 and CD206 in prostate tissue. (**I**) Immunofluorescence staining of CD86 and CD206 in prostate tissue. Scale bars, 50 μm. Data are presented as mean ± SD (n = 6 for A-I). *, $p < 0.05$; **, $p < 0.01$.

https://doi.org/10.2147/IJN.S596237

(Figure 4G-I), and downregulated pro-inflammatory cytokines in both serum and prostate tissue (Figure S2A and B, supplementary information). Thus, *L. john* alleviates CP/CPPS by limiting inflammatory cell recruitment and reducing pro-inflammatory mediators locally and systemically.

LjEVs Alleviate Prostate Inflammation and Inhibit M1 Macrophage Polarization in Alcohol-Fed EAP Mice

To investigate how *L. john* alleviates alcohol-aggravated CP/CPPS, extracellular vesicles were isolated from *L. john* for subsequent experiments. First, the isolated LjEVs were characterized using transmission electron microscopy (TEM) and nano-flow cytometry (nFCM). TEM imaging revealed that the extracted vesicles exhibited a classic circular or spherical morphology with a bilayered membrane structure (Figure 5A). The nFCM results demonstrated that the particle size was primarily distributed within the range of 30–150 nm, with an average diameter of 82.1 nm and a concentration of 2.13×10^{10} particles/mL (Figure 5B and 5C). We then performed an in vivo tracing study by intravenously administering indocyanine green (ICG)-labeled LjEVs to mice and monitoring their systemic distribution. The results showed that LjEVs were successfully delivered and accumulated in the prostate, with ex vivo fluorescence imaging revealing significantly higher prostate fluorescence intensity in the LjEVs group compared to the free ICG control group (Figure 5D and 5E).

We next evaluated the therapeutic effect of LjEVs on alcohol-fed EAP mice. LjEVs treatment significantly reduced the response frequency to mechanical stimuli in the pelvic region (Figure 5F), raised the 50% withdrawal threshold (Figure 5G), and alleviated prostate tissue inflammation (Figure 5H and I). Furthermore, it decreased $CD45^+$ leukocyte infiltration in the prostate (Figure 5J and K), inhibited M1 macrophage polarization and promoted M2 macrophage polarization (Figure 5L and M), and lowered the levels of pro-inflammatory cytokines in the serum as well as their gene expression in prostate tissue (Figure 5N and O). These findings demonstrate that LjEVs mitigate prostatic inflammation and inhibit M1 macrophage polarization in alcohol-fed EAP mice.

LjEVs Inhibit Both M1 Macrophage Polarization and the TNF-α/NF-κB Signaling Pathway in RAW 264.7 Cells

Building on the above findings that LjEVs alleviate alcohol-aggravated CP/CPPS, we sought to elucidate whether this protective effect is mediated through the modulation of macrophage polarization. To visualize cellular uptake, we labeled LjEVs with the fluorescent membrane dye Dil (forming EVs@Dil). RAW 264.7 cells were then incubated with either free DiI or EVs@Dil for 12 hours. Confocal microscopy revealed distinct fluorescent puncta within the cells incubated with EVs@Dil, indicating that RAW 264.7 cells internalize LjEVs (Figure 6A).

To investigate whether LjEVs exert an immunomodulatory effect on macrophages, RAW 264.7 cells were stimulated with LPS in the presence or absence of LjEVs. qRT-PCR analysis revealed that LjEVs significantly downregulated the expression of key inflammatory cytokines (IL-1β, IL-6, TNF-α) and the M1 macrophage marker (iNOS), while upregulating the M2 macrophage marker (Arg-1) (Figure 6C). This change in polarization was corroborated by flow cytometry, which showed a decrease in the M1 macrophage population and a concomitant increase in the M2 population following LjEVs intervention (Figure 6D). Consistent with these findings, LjEVs treatment also markedly reduced LPS-induced nitric oxide (NO) production (Figure 6G).

To elucidate the underlying mechanism, we performed transcriptomic sequencing on cells from different treatment groups. KEGG pathway enrichment analysis of the differentially expressed genes highlighted the pivotal role of the TNF-α/NF-κB signaling pathway (Figure 6B). Western blot validation confirmed that LjEVs intervention effectively suppressed the activation of this pathway (Figure 6E and F). Furthermore, we extracted proteins from mouse prostate tissue for Western blot analysis. The results revealed that the activity of the TNF-α/NF-κB signaling pathway was significantly altered following alcohol intervention, gut microbiota transplantation, and treatment with either *L. john* or LjEVs (Figure S3A–H, supplementary information). Collectively, these results suggest that LjEVs inhibit M1 macrophage polarization and pro-inflammatory gene expression in RAW 264.7 cells, potentially through the inhibition of the TNF-α/NF-κB pathway; furthermore, this pathway is likely to play a central role in the context of alcohol-exacerbated CP/CPPS.

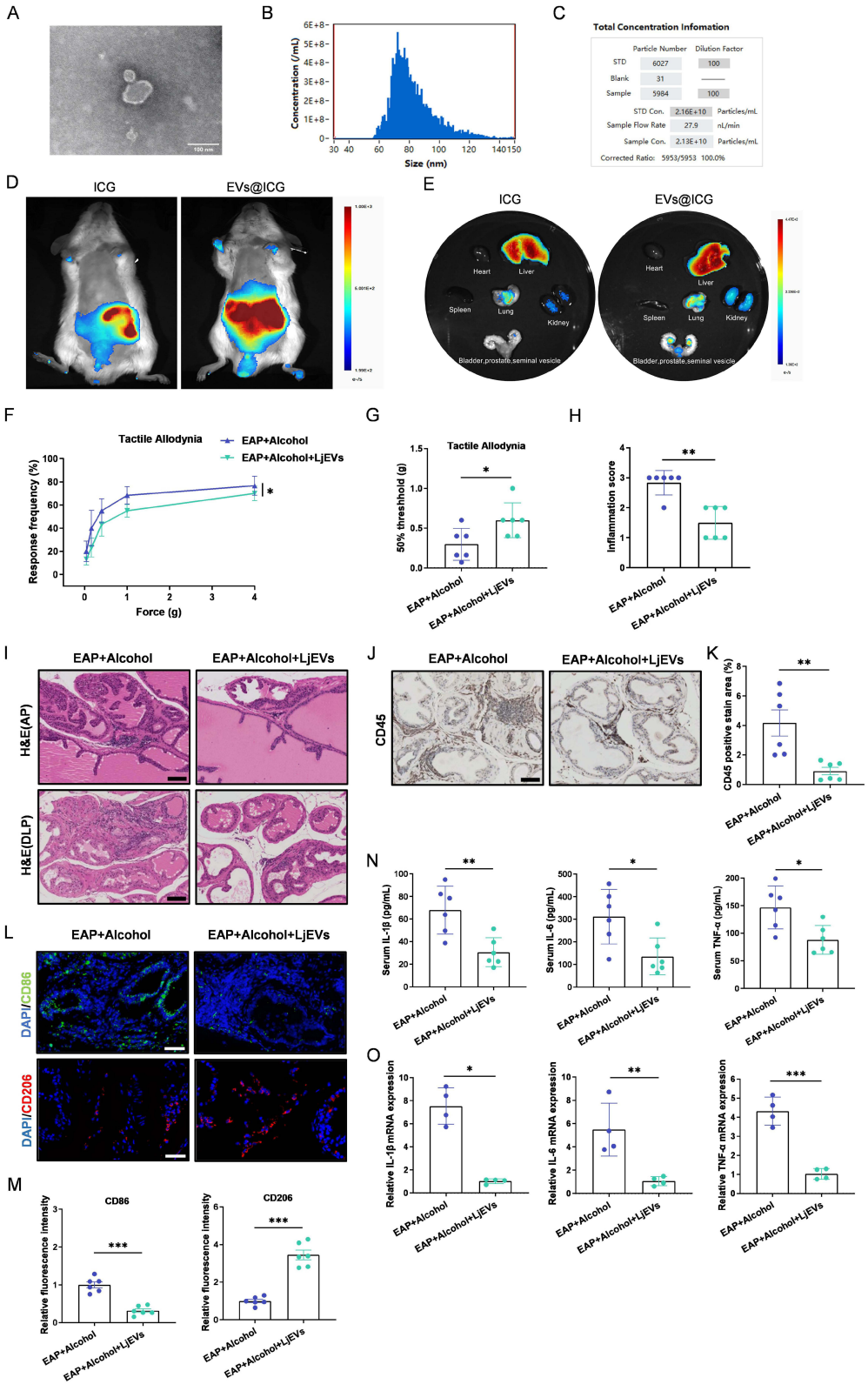

Figure 5 LjEVs alleviate prostate inflammation and inhibit M1 macrophage polarization in EAP mice. (**A**) Transmission electron microscopy (TEM) image of LjEVs. Scale bars, 100 nm. (**B** and **C**) Size distribution and concentration of LjEVs analyzed by nano-flow cytometry (nFCM). (**D** and **E**) The biodistribution of EVs@ICG versus free ICG was assessed in vivo and ex vivo after administration via tail vein injection. (**F** and **G**) Response frequency to mechanical stimuli and the 50% mechanical withdrawal threshold. (**H**) Prostate inflammation score. (**I**) H&E staining of the anterior and dorsolateral prostate. Scale bars, 100 μm. (**J**) Immunohistochemical staining of CD45 in prostate tissues. Scale bars, 100 μm. (**K**) Percentage of CD45-positive staining in prostate immunohistochemistry. (**L**) Immunofluorescence staining of CD86 and CD206 in prostate tissue. Scale bars, 50 μm. (**M**) Relative fluorescence intensity of CD86 and CD206 in prostate tissue. (**N**) Pro-inflammatory cytokine levels in serum. (**O**) Pro-inflammatory cytokine mRNA expression in prostate tissues. Data are presented as mean ± SD (n = 6 for F-N, n = 4 for O). *, $p < 0.05$; **, $p < 0.01$; ***, $p < 0.001$.

https://doi.org/10.2147/IJN.S596237

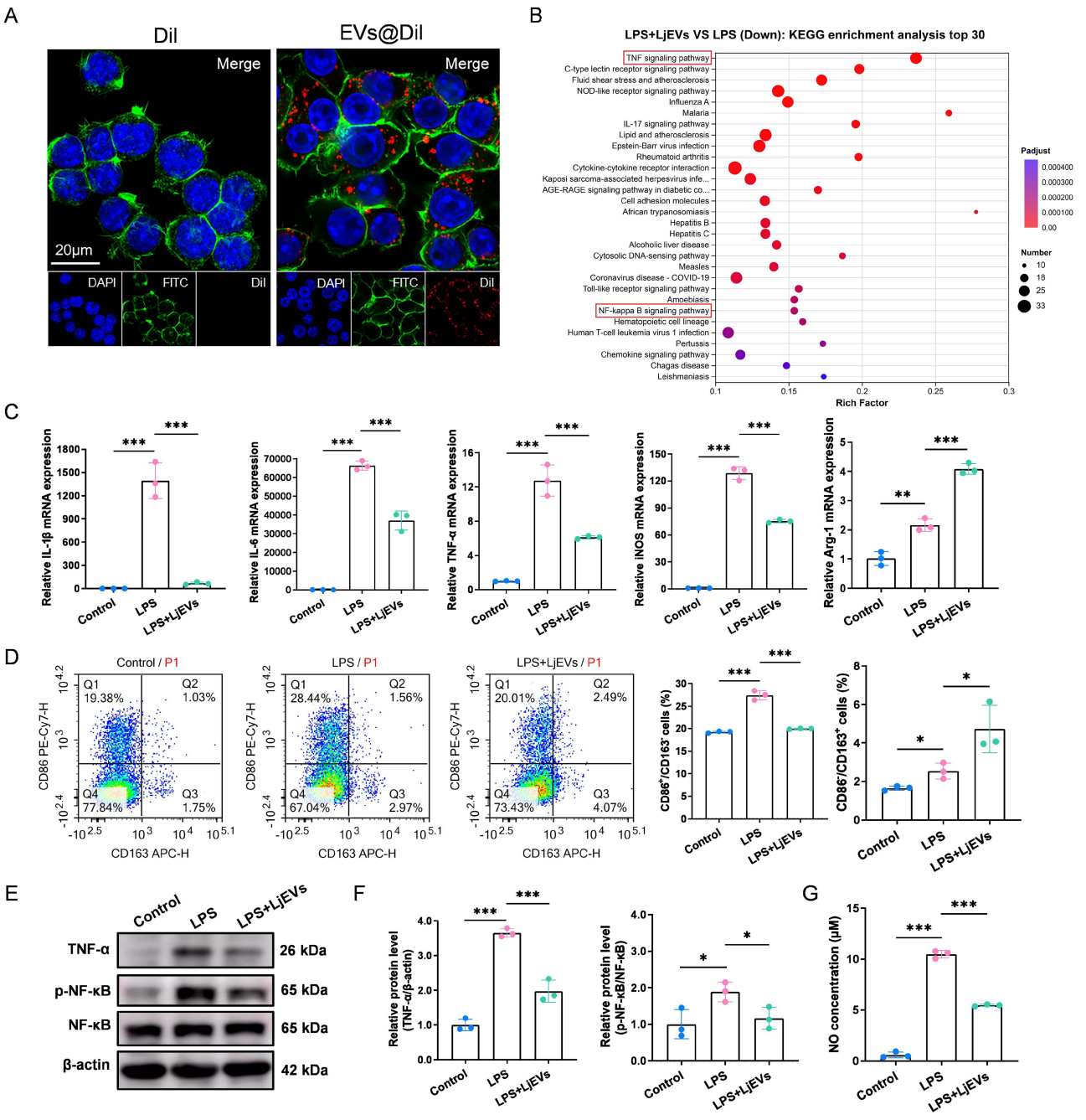

Figure 6 LjEVs inhibit both M1 macrophage polarization and the TNF-α/NF-κB signaling pathway in RAW 264.7 cells. (**A**) Uptake of EVs@DiI or DiI alone by RAW 264.7 cells after co-incubation was analyzed using confocal microscopy. Nuclei were stained with DAPI, and the cytoskeleton was stained with FITC-phalloidin. Scale bars, 20 μm. (**B**) KEGG pathway enrichment analysis based on transcriptomic sequencing data from the LPS group and the LPS+LjEVs group. The enriched TNF-α/NF-kB signaling pathway is highlighted with a red box in the figure. (**C**) qRT-PCR analysis of M1/M2 macrophage marker gene expression (IL-1β, IL-6, TNF-α, iNOS, Arg-1) in RAW 264.7 cells. (**D**) Flow cytometry analysis of M1/M2 macrophage polarization (CD86/CD163) across different groups. (**E-F**) Western blot analysis of protein expression in the TNF-α/NF-κB pathway across different groups. (**G**) NO concentration (determined as nitrite) in each group was quantified using the Griess reagent assay. Data are presented as mean ± SD (n = 3 for B-G). *, $p < 0.05$; **, $p < 0.01$; ***, $p < 0.001$.

Exogenous TNF-α Reverses the Inhibitory Effect of LjEVs on M1 Macrophage Polarization

To verify whether the TNF-α/NF-κB signaling pathway mediates the inhibition of M1 macrophage polarization by LjEVs, we employed recombinant TNF-α as a pathway activator. We first confirmed that TNF-α treatment effectively reversed the inhibitory effect of LjEVs on the TNF-α/NF-κB pathway (Figure 7E–F). Subsequently, qRT-PCR analysis

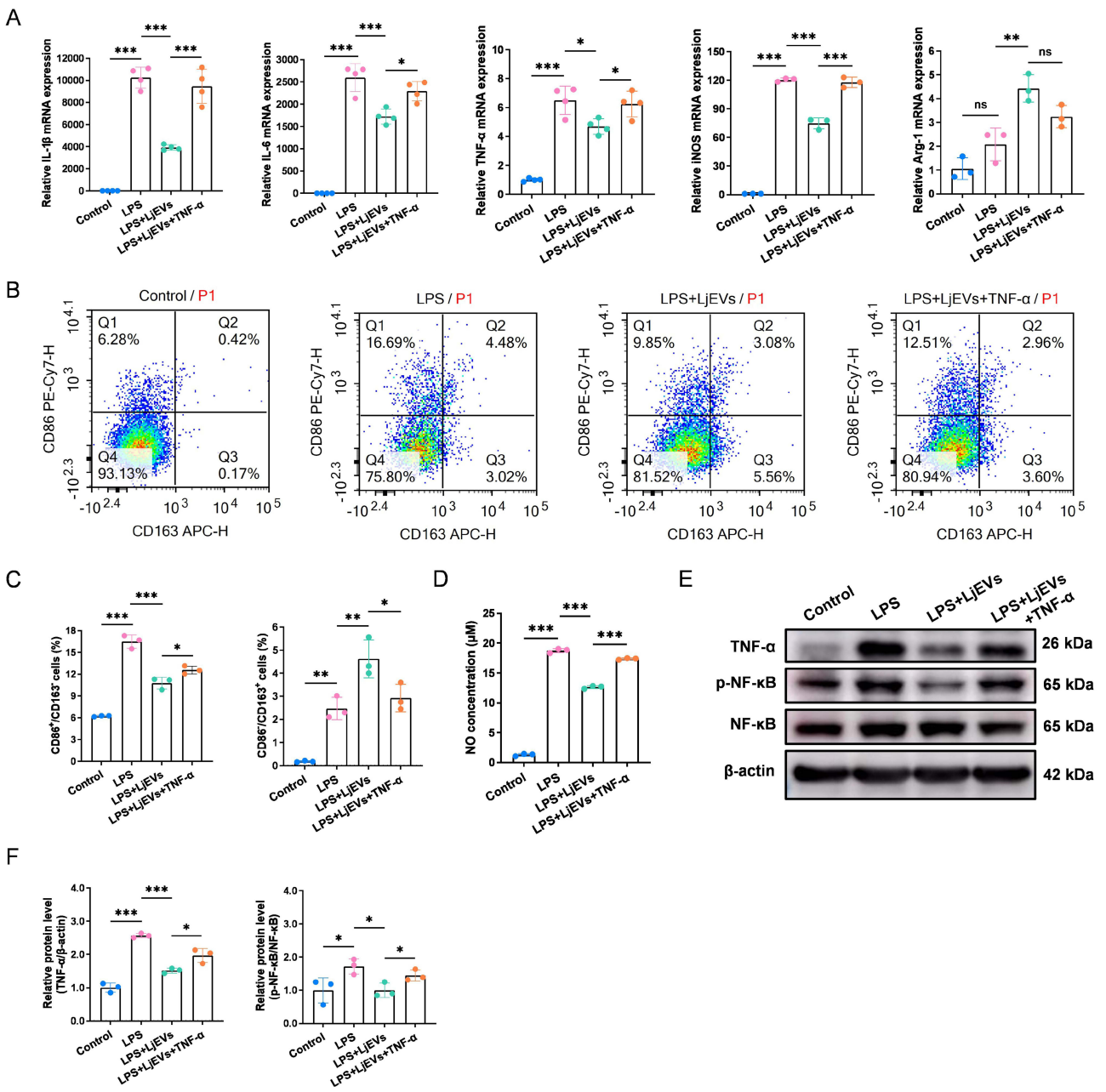

Figure 7 Exogenous TNF-α reverses the inhibitory effect of LjEVs on M1 macrophage polarization. (**A**) qRT-PCR analysis of M1/M2 macrophage marker gene expression (IL-1β, IL-6, TNF-α, iNOS, Arg-1) in RAW 264.7 cells. (**B** and **C**) Flow cytometry analysis of M1/M2 macrophage polarization (CD86/CD163) across different groups. (**D**) NO concentration (determined as nitrite) in each group was quantified using the Griess reagent assay. (**E** and **F**) Western blot analysis of protein expression in the TNF-α/NF-κB pathway across different groups. Data are presented as mean ± SD (n = 3-4 for A-F). *, $p < 0.05$; **, $p < 0.01$; ***, $p < 0.001$.
Abbreviation: ns, not significant.

showed that recombinant TNF-α up-regulated the gene expression of pro-inflammatory cytokines and M1 markers (Figure 7A). This shift toward a pro-inflammatory phenotype was corroborated by flow cytometry, which revealed an increase in the M1 macrophage population and a decrease in the M2 population (Figure 7B and C). Consistent with these changes, NO concentration was also elevated (Figure 7D). Taken together, these results demonstrate that the TNF-α/NF-κB pathway at least partially mediates the inhibitory effect of LjEVs on M1 macrophage polarization.

https://doi.org/10.2147/IJN.S596237

Discussion

In summary, we found that alcohol consumption exacerbated EAP in mice, as evidenced by increased prostatic inflammation, pelvic pain, and M1 macrophage polarization. Notably, the gut microbiota appeared to mediate this effect, and the abundance of *L. john* was reduced in alcohol-fed EAP mice. Supplementation with *L. john* or its extracellular vesicles (LjEVs) alleviated the condition. In vitro, LjEVs suppressed M1 macrophage polarization and pro-inflammatory responses, potentially via the TNF-α/NF-κB pathway. Consistent with previous EAP studies, alcohol exacerbated CP/CPPS,[18,46] but our study further identifies LjEVs as a novel protective agent modulating macrophage polarization. These findings provide experimental insights into the gut–prostate axis and suggest a potential therapeutic strategy for CP/CPPS.

Extensive research indicates that alcohol consumption impacts the progression of inflammatory diseases. For example, chronic alcohol exposure induces gut microbiota dysbiosis, characterized by an increase in pathogenic bacteria and a decrease in commensal bacteria. This dysbiosis can directly contribute to liver injury through mechanisms such as increased production of exotoxins, or indirectly by disrupting the intestinal barrier, stimulating pro-inflammatory pathways, and altering bile acid homeostasis, collectively exacerbating hepatic inflammation and damage.[47] In this study, we have shown that alcohol exacerbates inflammation and pain in EAP mice by modulating the gut microbiota. Additionally, alcohol metabolism generates reactive oxygen species (ROS) that can damage cellular structures, and its metabolite acetaldehyde can trigger inflammatory responses.[48] The integrity of the blood-prostate barrier, maintained by structures such as prostate epithelial cells, may be compromised, potentially allowing alcohol to penetrate and accumulate in prostate tissue. Therefore, it is possible that the gut microbiota is one mediator of alcohol's effects on CP/CPPS, and whether alcohol acts synergistically with these microbial changes to exacerbate the disease remains to be determined.

In healthy individuals, the gut microbiota contributes to intestinal homeostasis through multiple mechanisms. In contrast, in patients with inflammatory diseases, the balance between the gut microbiota and the host immune system is disrupted, and this dysbiosis can drive the onset and progression of chronic inflammation.[49,50] *L. john* is recognized as a key beneficial commensal in the gut, playing a significant role in maintaining host metabolic homeostasis, modulating immune responses, and supporting intestinal health.[35] In this study, the abundance of *L. john* in the feces of alcohol-fed EAP mice showed a decreased trend, while transplantation of *L. john* alleviated CP/CPPS. Extracellular vesicles derived from probiotics serve as important mediators in host immune responses and exhibit anti-inflammatory properties.[51] Bacterial EVs are spherical, nanosized vesicles with a diameter typically ranging from 20 to 400 nm. They carry a diverse cargo including DNA, RNA, lipids and proteins, enabling them to mediate microbiota-host communication.[28] Accumulating evidence indicates the anti-inflammatory role of LjEVs in modulating host immune responses.[52,53] In this study, administration of LjEVs to alcohol-fed EAP mice demonstrated their efficacy in alleviating both inflammation and pain. However, it is important to note that it remains unclear whether the benefits of *L. john* in alcohol-aggravated prostatitis are mediated exclusively by its extracellular vesicles or involve other mechanisms, such as the production of anti-inflammatory metabolites like short-chain fatty acids. This represents an important direction for future research. Nevertheless, our findings clearly demonstrate that supplementation with *L. john* or its extracellular vesicles presents a beneficial strategy for mitigating alcohol-exacerbated CP/CPPS.

Macrophages play a pivotal role in the pathogenesis of CP/CPPS. While their activation is crucial, targeting and inhibiting M1 macrophage polarization has emerged as a promising therapeutic strategy to alleviate the condition.[54] Consistent with this, our results showed that alcohol feeding in EAP mice led to aggravated prostate inflammation and an increased presence of M1 macrophages. Supplementation with *L. john* or its extracellular vesicles reversed these alterations, reducing both inflammation and M1 macrophage infiltration. To explore the underlying mechanism, RAW 264.7 cells were treated with LPS alone or in combination with LjEVs, and the responses were compared. We found that LjEVs inhibited M1 macrophage polarization and reduced the expression of pro-inflammatory cytokines. Furthermore, transcriptomic sequencing analysis suggested the TNF-α/NF-κB pathway as a key signaling axis, which is a well-established core target in treating various inflammatory diseases.[55,56] Subsequent experiments verified that LjEVs suppress M1 macrophage polarization and downregulate inflammatory gene expression by inhibiting the TNF-α/NF-κB signaling pathway. Furthermore, the altered activity of the TNF-α/NF-κB pathway across the disease model is associated with the disease.

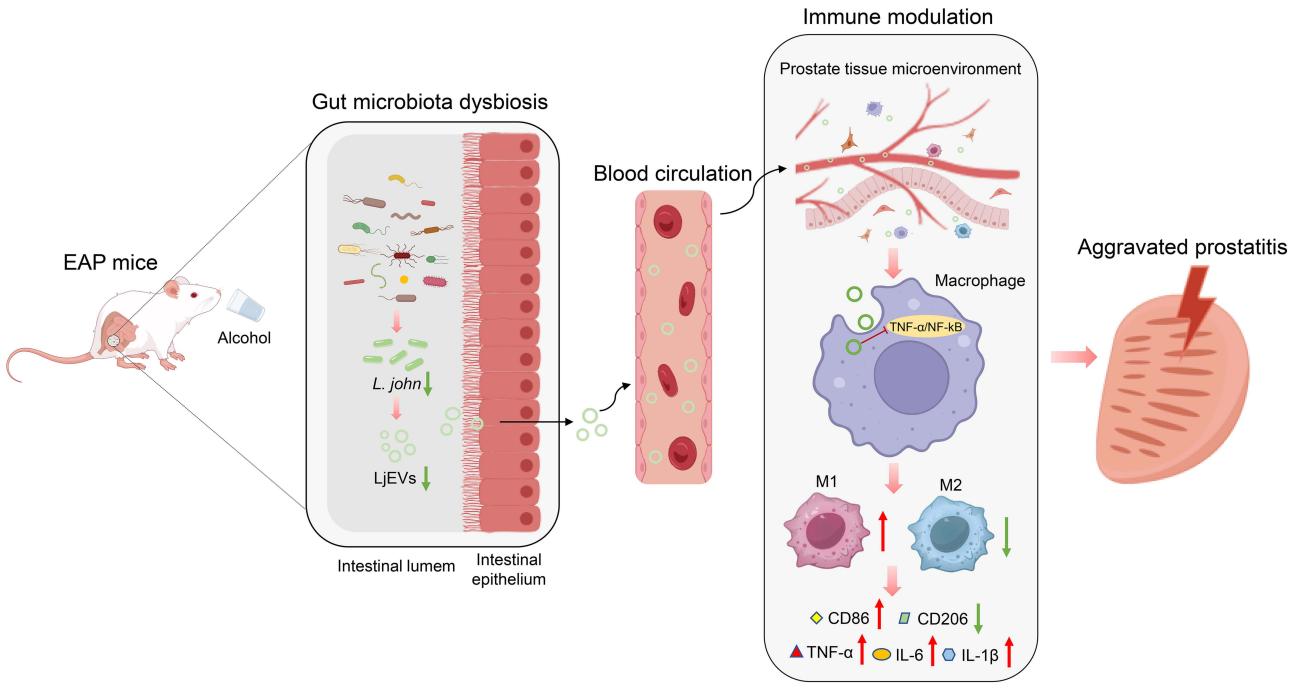

Figure 8 Graphical summary of the major findings. Upward arrow (↑) indicates upregulation, downward arrow (↓) indicates downregulation. The red "—|" symbol indicates inhibition of the corresponding pathway.
Abbreviations: EAP, experimental autoimmune prostatitis; *L. john, Lactobacillus johnsonii*; LjEVs, *Lactobacillus johnsonii*-derived extracellular vesicles.

This study has several limitations. First, because our experiments were limited to a mouse model of EAP, the present findings are mechanistic and their implications for human therapy remain to be determined. Second, we did not perform macrophage depletion or pathway-specific inhibition experiments in EAP mice; therefore, definitive causal evidence for the role of macrophages in mediating alcohol's effects on CP/CPPS could not be established. Third, the role of LjEVs as the sole mediator of the protective effects of *L. john* remains inferential, as other probiotic-derived metabolites were not excluded and may also contribute to the observed benefits. Fourth, although microbiota dependence is supported by FMT experiments, broader compositional shifts beyond *L. john* could also contribute to the phenotype. Despite these limitations, the study provides a coherent and mechanistically informed framework linking alcohol-induced gut dysbiosis, LjEVs, and macrophage polarization in the context of CP/CPPS.

Conclusion

This study demonstrated that alcohol exacerbated EAP by reducing *L. john*, which in turn promoted prostatic M1 macrophage polarization via the TNF-α/NF-κB pathway (Figure 8). Supplementation with *L. john* or LjEVs ameliorated the disease by suppressing this pathway, offering a microbiota-targeted therapy for alcohol-aggravated CP/CPPS.

Abbreviations

CP/CPPS, chronic prostatitis/chronic pelvic pain syndrome; EAP, experimental autoimmune prostatitis; FMT, fecal microbiota transplantation; *L. john, Lactobacillus johnsonii*; LjEVs, *Lactobacillus johnsonii*-derived extracellular vesicles; CFU, colony forming units; PBS, phosphate buffered saline; H&E, hematoxylin and eosin; WB, Western blot; qRT-PCR, quantitative real-time polymerase chain reaction; TEM, transmission electron microscopy; nFCM, nanoflow cytometry; LPS, lipopolysaccharide; SD, standard deviation.

Data Sharing Statement

The data will be available upon reasonable request to the corresponding author, Binbin Gong.

Ethics Approval and Informed Consent

Clinical trial number: not applicable. All animal experiments comply with guidelines for the care and use of laboratory animals. The experimental protocols were approved by the Animal Ethics Committee of the First Affiliated Hospital of Nanchang University (CDYFY-IACUC-202311QR006).

Acknowledgments

We thank OE Biotech Co., Ltd. (Shanghai, China) for technical support in fecal 16S rRNA sequencing.

Funding

This work was supported by the following grants: the National Natural Science Foundation of China (82460159), the Jiangxi Provincial Natural Science Foundation (20252BAC240562).

Disclosure

The authors declare no conflicts of interest in this work.

References

1. Deng GC, Lu M, Zhao YY, Yuan Y, Chen G. Activated spinal astrocytes contribute to the later phase of carrageenan-induced prostatitis pain. *J Neuroinflamm*. 2019;16(1):189. doi:10.1186/s12974-019-1584-3
2. Liu SJ, Guo BD, Gao QH, et al. Ursolic acid alleviates chronic prostatitis via regulating NLRP3 inflammasome-mediated Caspase-1/GSDMD pyroptosis pathway. *Phytother Res*. 2024;38(1):82–97. doi:10.1002/ptr.8034
3. Polackwich AS, Shoskes DA. Chronic prostatitis/chronic pelvic pain syndrome: a review of evaluation and therapy. *Prostate Cancer Prostatic Dis*. 2016;19(2):132–138. doi:10.1038/pcan.2016.8
4. Hua X, Ge S, Zhang M, et al. Pathogenic roles of CXCL10 in experimental autoimmune prostatitis by modulating macrophage chemotaxis and cytokine secretion. *Front Immunol*. 2021;12:706027. doi:10.3389/fimmu.2021.706027
5. Motrich RD, Breser ML, Molina RI, Tissera A, Olmedo JJ, Rivero VE. Patients with chronic prostatitis/chronic pelvic pain syndrome show T helper type 1 (Th1) and Th17 self-reactive immune responses specific to prostate and seminal antigens and diminished semen quality. *BJU Int*. 2020;126(3):379–387. doi:10.1111/bju.15117
6. Zhang F, Meng T, Feng R, et al. MIF aggravates experimental autoimmune prostatitis through activation of the NLRP3 inflammasome via the PI3K/AKT pathway. *Int Immunopharmacol*. 2024;141:112891. doi:10.1016/j.intimp.2024.112891
7. Liu Z, Murphy SF, Wong L, Schaeffer AJ, Thumbikat P. Neuronal/astrocytic expression of chemokine (C-C motif) ligand 2 is associated with monocyte/macrophage recruitment in male chronic pelvic pain. *Pain*. 2020;161(11):2581–2591. doi:10.1097/j.pain.0000000000001954
8. Hua X, Zhang J, Ge S, et al. CXCR3 antagonist AMG487 ameliorates experimental autoimmune prostatitis by diminishing Th1 cell differentiation and inhibiting macrophage M1 phenotypic activation. *Prostate*. 2022;82(13):1223–1236. doi:10.1002/pros.24395
9. Wang Y, Guan Y, Feng D, et al. Infiltrating macrophages replace Kupffer cells and play diverse roles in severe alcohol-associated hepatitis. *Cell Mol Immunol*. 2025;22(10):1262–1275. doi:10.1038/s41423-025-01343-1
10. Danpanichkul P, Pang Y, Kim D, et al. Disproportionately rising mortality rates of alcohol-associated acute pancreatitis: analysis from centers for disease control and prevention database (2011-2020). *Pancreatology*. 2025;25(4):508–515. doi:10.1016/j.pan.2025.05.012
11. Zhou T, Im PK, Hariri P, et al. Associations of alcohol intake with subclinical carotid atherosclerosis in 22,000 Chinese adults. *Atherosclerosis*. 2023;377:34–42. doi:10.1016/j.atherosclerosis.2023.06.012
12. Song J, She J, Yin J, Hu S, Shi G, Chang L. Impact of alcohol consumption on atherosclerosis: a systematic review and meta-analysis. *Front Nutr*. 2025;12:1563759. doi:10.3389/fnut.2025.1563759
13. Lowe PP, Morel C, Ambade A, et al. Chronic alcohol-induced neuroinflammation involves CCR2/5-dependent peripheral macrophage infiltration and microglia alterations. *J Neuroinflamm*. 2020;17(1):296. doi:10.1186/s12974-020-01972-5
14. Xu J, Lai KKY, Verlinsky A, et al. Synergistic steatohepatitis by moderate obesity and alcohol in mice despite increased adiponectin and p-AMPK. *J Hepatol*. 2011;55(3):673–682. doi:10.1016/j.jhep.2010.12.034
15. Chen X, Hu C, Peng Y, et al. Association of diet and lifestyle with chronic prostatitis/chronic pelvic pain syndrome and pain severity: a case-control study. *Prostate Cancer Prostatic Dis*. 2016;19(1):92–99. doi:10.1038/pcan.2015.57
16. Zhang J, Zhang X, Cai Z, Li N, Li H. The lifetime risk and prognosis of chronic prostatitis/chronic pelvic pain syndrome in the middle-aged chinese males. *Am J Men's Health*. 2019;13(4):1557988319865380. doi:10.1177/1557988319865380
17. Liu C, Yue S, Niu D, et al. Alcohol intake-induced aggravation of chronic prostatitis/chronic pelvic pain syndrome is associated with reduced gut microbiota-driven short-chain fatty acid propionate and butyrate. *World J Men's Health*. 2025. doi:10.5534/wjmh.240223
18. Du HX, Yue SY, Niu D, et al. Alcohol intake exacerbates experimental autoimmune prostatitis through gut microbiota driving cholesterol biosynthesis-mediated Th17 differentiation. *Int Immunopharmacol*. 2024;139:112669. doi:10.1016/j.intimp.2024.112669
19. Xu S, Chen J, Yue S, et al. Alcohol intake exacerbates experimental autoimmune prostatitis through activating PI3K/AKT/mTOR pathway-mediated Th1 differentiation. *Front Immunol*. 2024;15:1512456. doi:10.3389/fimmu.2024.1512456
20. Shoskes DA, Wang H, Polackwich AS, Tucky B, Altemus J, Eng C. Analysis of gut microbiome reveals significant differences between men with chronic prostatitis/chronic pelvic pain syndrome and controls. *J Urol*. 2016;196(2):435–441. doi:10.1016/j.juro.2016.02.2959
21. Konkol Y, Keskitalo A, Vuorikoski H, et al. Chronic nonbacterial prostate inflammation in a rat model is associated with changes of gut microbiota that can be modified with a galactoglucomannan-rich hemicellulose extract in the diet. *BJU Int*. 2019;123(5):899–908. doi:10.1111/bju.14553

22. Du HX, Yue SY, Niu D, et al. Gut microflora modulates Th17/Treg cell differentiation in experimental autoimmune prostatitis via the short-chain fatty acid propionate. *Front Immunol*. 2022;13:915218. doi:10.3389/fimmu.2022.915218
23. Wang X, Yue SY, Chen L, et al. Lycium barbarum polysaccharides alleviate experimental autoimmune prostatitis by putrescine/TRAF/JAK/STAT-mediated Th17 differentiation. *Phytomedicine*. 2025;147:157210. doi:10.1016/j.phymed.2025.157210
24. Mercado-Monroy J, Falfán-Cortés RN, Muñóz-Pérez VM, Gómez-Aldapa CA, Castro-Rosas J. Probiotics as modulators of intestinal barrier integrity and immune homeostasis: a comprehensive review. *J Sci Food Agri*. 2026;106(5):2578–2590. doi:10.1002/jsfa.70168
25. Liu HY, Yuan P, Li S, et al. *Lactobacillus johnsonii* alleviates experimental colitis by restoring intestinal barrier function and reducing NET-mediated gut-liver inflammation. *Commun Biol*. 2025;8(1):1222. doi:10.1038/s42003-025-08679-4
26. Yang YSH, Chou HC, Chen CM. Maternal *Lactobacillus johnsonii* supplementation attenuates hyperoxia-induced lung injury in neonatal mice through microbiota regulation. *Pediatrics Neonatol*. 2025;66(4):382–389. doi:10.1016/j.pedneo.2024.09.005
27. Yin R, Wang T, Sun J, et al. Postbiotics from *Lactobacillus johnsonii* activates gut innate immunity to mitigate alcohol-associated liver disease. *Adv Sci*. 2025;12(2):e2405781. doi:10.1002/advs.202405781
28. Nie X, Li Q, Chen X, Onyango S, Xie J, Nie S. Bacterial extracellular vesicles: vital contributors to physiology from bacteria to host. *Microbiolog Res*. 2024;284:127733. doi:10.1016/j.micres.2024.127733
29. González-Lozano E, García-García J, Gálvez J, et al. Novel horizons in postbiotics: lactobacillaceae extracellular vesicles and their applications in health and disease. *Nutrients*. 2022;14(24):5296. doi:10.3390/nu14245296
30. Guo J, Huang Z, Wang Q, et al. Opportunities and challenges of bacterial extracellular vesicles in regenerative medicine. *J Nanobiotechnol*. 2025;23(1):4. doi:10.1186/s12951-024-02935-1
31. Tao S, Song M, Fan J, Zhu F, Lv T, Wei H. *Lactobacillus johnsonii*-derived extracellular vesicles carrying GAPDH protect against ulcerative colitis through modulating macrophage polarization. *J Adv Res*. 2025;69:545–563. doi:10.1016/j.jare.2025.06.035
32. Tao S, Fan J, Li J, et al. Extracellular vesicles derived from *Lactobacillus johnsonii* promote gut barrier homeostasis by enhancing M2 macrophage polarization. *J Adv Res*. 2025;69:545–563. doi:10.1016/j.jare.2024.03.011
33. Liu R, Zhou Y, Chen H, et al. Membrane vesicles from *Lactobacillus johnsonii* delay osteoarthritis progression via modulating macrophage glutamine synthetase/mTORC1 axis. *Biomed Pharmacother*. 2023;165:115204. doi:10.1016/j.biopha.2023.115204
34. Jia DJ, Wang QW, Hu YY, et al. *Lactobacillus johnsonii* alleviates colitis by TLR1/2-STAT3 mediated CD206(+) macrophages(IL-10) activation. *Gut Microbes*. 2022;14(1):2145843. doi:10.1080/19490976.2022.2145843
35. Cai Y, Huang Y, Wang Y, Lin C, Qiu L, Wei H. *Lactobacillus johnsonii* GLJ001 prevents DSS-induced colitis in mice by inhibiting M1 macrophage polarization via gut microbiota-SCFAs axis. *Int Immunopharmacol*. 2025;144:113671. doi:10.1016/j.intimp.2024.113671
36. Liu YF, Xie WJ, Xi P, et al. Astaxanthin alleviates chronic prostatitis/chronic pelvic pain syndrome by increasing colonization of Akkermansia muciniphila in the intestine. *Phytomedicine*. 2024;123:155249. doi:10.1016/j.phymed.2023.155249
37. Bertola A, Mathews S, Ki SH, Wang H, Gao B. Mouse model of chronic and binge ethanol feeding (the NIAAA model). *Nat Protocols*. 2013;8(3):627–637. doi:10.1038/nprot.2013.032
38. Peng X, Li F, Xia L, Lu M. Macrophage heterogeneity regulation by small extracellular vesicles from adipose-derived stem cells: a promising approach for treating chronic prostatitis/pelvic pain syndrome. *Biomat Adv*. 2025;166:214066. doi:10.1016/j.bioadv.2024.214066
39. Quick ML, Done JD, Thumbikat P. Measurement of tactile allodynia in a murine model of bacterial prostatitis. *J Visual Exp* 2013;(71):e50158. doi:10.3791/50158
40. Chaplan SR, Bach FW, Pogrel JW, Chung JM, Yaksh TL. Quantitative assessment of tactile allodynia in the rat paw. *J Neurosci Meth*. 1994;53(1):55–63. doi:10.1016/0165-0270(94)90144-9
41. Breser ML, Motrich RD, Sanchez LR, Rivero VE. Chronic pelvic pain development and prostate inflammation in strains of mice with different susceptibility to experimental autoimmune prostatitis. *Prostate*. 2017;77(1):94–104. doi:10.1002/pros.23252
42. Jing B, Gao Y, Wang L, et al. Probiotic membrane vesicles ameliorate atherosclerotic plaques by promoting lipid efflux and polarization of foamy macrophages. *J Nanobiotechnol*. 2025;23(1):296. doi:10.1186/s12951-025-03360-8
43. Rivero VE, Cailleau C, Depiante-Depaoli M, Riera CM, Carnaud C. Non-obese diabetic (NOD) mice are genetically susceptible to experimental autoimmune prostatitis (EAP). *J Autoimmun*. 1998;11(6):603–610. doi:10.1006/jaut.1998.0248
44. Chen NW, Jin J, Xu H, et al. Effect of thermophilic bacterium HB27 manganese superoxide dismutase in a rat model of chronic prostatitis/chronic pelvic pain syndrome (CP/CPPS). *Asian J Androl*. 2022;24(3):323–331. doi:10.4103/aja202157
45. Jin C, Zhang F, Luo H, et al. The CCL5/CCR5/SHP2 axis sustains Stat1 phosphorylation and activates NF-κB signaling promoting M1 macrophage polarization and exacerbating chronic prostatic inflammation. *Cell Commun Signal*. 2024;22(1):584. doi:10.1186/s12964-024-01943-w
46. Zhang LG, Chen J, Meng JL, et al. Effect of alcohol on chronic pelvic pain and prostatic inflammation in a mouse model of experimental autoimmune prostatitis. *Prostate*. 2019;79(12):1439–1449. doi:10.1002/pros.23866
47. Jew MH, Hsu CL. Alcohol, the gut microbiome, and liver disease. *J Gastroenterol Hepatol*. 2023;38(8):1205–1210. doi:10.1111/jgh.16199
48. Kong EQZ, Subramaniyan V, Lubau NSA. Uncovering the impact of alcohol on internal organs and reproductive health: exploring TLR4/NF-kB and CYP2E1/ROS/Nrf2 pathways. *Animal Models Exp Med*. 2024;7(4):444–459. doi:10.1002/ame2.12436
49. White Z, Cabrera I, Kapustka I, Sano T. Microbiota as key factors in inflammatory bowel disease. *Front Microbiol*. 2023;14:1155388. doi:10.3389/fmicb.2023.1155388
50. Chen J, Chen B, Lin B, et al. The role of gut microbiota in prostate inflammation and benign prostatic hyperplasia and its therapeutic implications. *Heliyon*. 2024;10(19):e38302. doi:10.1016/j.heliyon.2024.e38302
51. Chen Q, Fang Z, Yang Z, et al. Lactobacillus plantarum-derived extracellular vesicles modulate macrophage polarization and gut homeostasis for alleviating ulcerative colitis. *J Agri Food Chem*. 2024;72(26):14713–14726. doi:10.1021/acs.jafc.4c01758
52. Zhao H, Yue N, Mai Z, et al. *Lactobacillus johnsonii*-derived extracellular vesicles restore mucosal immunity via taurine-linked Th17/Treg and IgA/IgG regulation in colitis. *J Nanobiotechnol*. 2025;23(1):612. doi:10.1186/s12951-025-03702-6
53. Li Z, Li M, Fang X, Yu D, Hu X. Dietary *Lactobacillus johnsonii*-derived extracellular vesicles ameliorate acute colitis by regulating gut microbiota and maintaining intestinal barrier homeostasis. *Food Funct*. 2024;15(23):11757–11779. doi:10.1039/d4fo04194a
54. Meng T, Zhang Y, Wang H, et al. Irf7 aggravates prostatitis by promoting Hif-1α-mediated glycolysis to facilitate M1 polarization. *Cell Mol Life Sci*. 2025;82(1):90. doi:10.1007/s00018-025-05608-w

55. Liu B, Yang F, Pu X, Yu J, Wang Q. TNF/NF-κB signaling pathway is involved in mechanisms of tongluo decoction on rat models with sequelae of pelvic inflammatory disease. *J Inflamm Res*. 2025;18:12949–12960. doi:10.2147/jir.S518734
56. Zhang Y, Zhang S, Liao P, et al. 3D hESC Exosome-Derived Circular RNA hsa_circ_0076798 Inhibits M1 Macrophage Inflammatory Response and Alleviates Liver Fibrosis by Suppressing TNF/NF-κB Pathway Through miR-1184/DICER1 Axis. *Biotechnol Bioeng*. 2025;122 (11):3073–3089. doi:10.1002/bit.70047